Developments in the Built Environment 15 (2023) 100197

Contents lists available at ScienceDirect

Developments in the Built Environment

journal homepage: www.sciencedirect.com/journal/developments-in-the-built-environment

Mechanical and durability performance of sustainable concretes containing conventional and emerging supplementary cementitious materials

Jin-Cheng Liu [a], Md. Uzzal Hossain [a], Dongxing Xuan [b], Hafiz Asad Ali [b], S. Thomas Ng [c,*], Hailong Ye [a,**]

[a] Department of Civil Engineering, The University of Hong Kong, Pokfulam Road, Hong Kong
[b] Department of Civil and Environmental Engineering, The Hong Kong Polytechnic University, Hung Hom, Hong Kong
[c] Department of Architecture and Civil Engineering, City University of Hong Kong, 83 Tat Chee Avenue, Kowloon Tong, Hong Kong

ARTICLE INFO

Keywords:
Natural pozzolan
Limestone calcined clay cement
Chloride diffusion
Water absorption
Alkali-silica reaction

ABSTRACT

This paper presents a comparative study on the mechanical and durability properties of concrete mixtures containing conventional supplementary cementitious materials (SCMs) and emerging alternatives (i.e., volcanic ash, volcanic ash-limestone blend, and metakaolin-limestone blend), with an emphasis on the latter. To enable effective comparison, identical volumetric substitution levels (30%) of SCMs along with a constant binder and aggregate volumes were employed. The metakaolin-limestone concrete performs the best among all types of concretes in terms of strength development, water absorption capacity and chloride penetration resistance. The incorporation of volcanic ash though reduces the compressive strength of concrete and increases water absorption capacity considerably compared to the reference Portland cement concrete, and its chloride diffusion coefficient is only about half of that of the reference concrete. In addition, the concretes containing volcanic ash or volcanic ash-limestone show better performance in controlling the potential alkali-silica reaction-induced expansion than the reference concrete and ground granulated blast-furnace slag concrete.

1. Introduction

Supplementary cementitious materials (SCMs) are being increasingly used in the concrete industry due to a shift towards the goal of high-performance and low-carbon. The SCMs, when used together with Portland cement, are beneficial to the durability of concrete and its long-term compressive strength. The SCMs commonly used in concrete include silica fume, pulverized fly ash (PFA), and ground granulated blast-furnace slag (GGBS), metakaolin (MK), among others (Gholampour et al., 2021; Gholampour and Ozbakkaloglu, 2017; de Brito and Kurda, 2021; da Silva Magalhães et al., 2023; Maddalena et al., 2021; Ashish et al., 2023). The PFA is a byproduct from the combustion of pulverized coal in coal-fired power plants, and the GGBS is a byproduct from the blast-furnaces used to make iron. Therefore, replacing Portland cement with PFA or GGBS in concrete can lower the environmental impact and resource consumption (Hafez et al., 2020; Fan and Miller, 2018; Nighot and Kumar, 2023), in addition to the benefits mentioned above.

However, the wide usage of PFA and GGBS in producing concrete has led to a shortage of these industrial by-products. The scarcity of PFA and GGBS will be further exacerbated in the future, with the ongoing endeavors in the transition towards greener way of producing electricity and steel. Therefore, there is an urgent need to find new alternative SCMs to produce sustainable concrete with comparable performance to those containing conventional SCMs. Recently, a blend of calcined kaolinite clay and limestone (LS) is added to Portland cement which forms the so-called limestone calcined clay cement (LC^3) (Scrivener et al., 2018; Nguyen et al., 2018, 2022). The blend of calcined clay, mainly in the form of MK, and LS can substitute clinker by up to 45 wt% in the LC^3 system, which can substantially lower the carbon footprint and overall impact on the environment associated with concrete products (Scrivener et al., 2018). The source materials of LC^3, i.e., the LS and kaolinite clay qualified for calcining, are abundant in many regions around the world, indicating the potential for large-scale LC^3 concrete production (Nickovic et al., 2012). Previous research has found that LC^3 concrete shows similar or better compressive strength and durability in a

* Corresponding author.
** Corresponding author.
E-mail addresses: thomasng@cityu.edu.hk (S.T. Ng), hlye@hku.hk (H. Ye).

https://doi.org/10.1016/j.dibe.2023.100197
Received 21 April 2023; Received in revised form 27 June 2023; Accepted 10 July 2023
Available online 11 July 2023

chloride-laden environment compared to its Portland cement counterpart, as a result of a denser microstructure of the LC^3 binder system (Dhandapani et al., 2018; Sharma et al., 2021; Du and Dai Pang, 2020).

Volcanic ash (VA) is another potentially alternative SCM for concrete (Al-Fadala et al., 2017; Siddique, 2012; Lemougna et al., 2018). Besides that, VA is also one key ingredient to reproduce ancient Roman concrete with exceptional durability performance (Jackson et al., 2010, 2014; Seymour et al., 2023). As compared to PFA and GGBS, VA is a natural pozzolana widely available in volcanic areas worldwide. And there is a steady supply of fresh sources of VA over time (Hossain and Lachemi, 2006, 2007). The effective exploitation of VA has the potential to transform it into a valuable natural resource capable of producing low-cost concrete materials, which, in the meantime, is advantageous to rehabilitation of volcanic disaster regions (Hossain et al., 2022). The utilization of volcanic ash as a SCM in concrete production has been investigated in several studies (Hossain and Lachemi, 2006, 2007; Meddah, 2015). In general, previous studies hold the common view that concrete possessing acceptable strength and durability properties can be developed with a maximum replacement of up to 20 wt% by VA. The addition of new SCMs, e.g., recycled waste glass, may induce potential alkali-silica reaction (ASR) expansion in concrete (Mehta and Ashish, 2020). The ASR, widely known as concrete cancer, can result in serious cracking in concrete, leading to critical structural problems. Hossain and Lachemi (2007) emphasized that the alkali-silica reactivity of VA concrete warrants investigations because of the existence of high alkali and aluminum oxide content in VA. Nevertheless, no test result on the alkali-silica reactivity of VA concrete was reported to the best of the authors' knowledge. Furthermore, the success of the LC^3 system demonstrates that limestone can be effectively utilized as SCM in tandem with calcined clay. The viability of VA-limestone blend as SCM in concrete is rarely reported and should therefore deserve a proper investigation.

Extensive studies have been conducted to study the mechanical and durability performance of concrete containing SCMs, especially for PFA and GGBS over the past decades (Elahi et al., 2010; Liu et al., 2022; De Maeijer et al., 2020; Tavasoli et al., 2018; Soutsos et al., 2020). But so far there is a lack of fair and direct comparisons on the effects of various SCMs, including the commonly used ones and the emerging ones, on the mechanical or durability properties of concrete. To fill in this research gap, this study investigated fresh, mechanical and durability properties of concretes containing two conventional SCMs and three emerging ones, all benchmarked against a reference Portland cement concrete. To enable fair and effective comparison, identical volumetric substitution levels (30%) of SCMs along with a constant binder and aggregate volumes were employed. The SCMs investigated in this study include GGBS, PFA, VA, VA-LS blend, and MK-LS blend (LC^3). The fresh and mechanical properties of concrete were characterized by initial and final setting time, compressive strength, flexural strength and splitting tensile strength, while the durability properties were characterized by rate of water absorption, alkali-silica reactivity, and bulk chloride diffusion tests. Therefore, the specific objectives of this study are (a) to directly compare setting time, mechanical and durability properties of concretes containing conventional and non-conventional SCMs, so as to support decision-making in adopting suitable SCMs for structural concrete catering to the needs of both strength and durability; (b) to assess the alkaline-silica reactivity of concrete with different SCMs, especially VA; and (c) to study the feasibility of blend of VA and LS as SCMs to produce workable, sustainable, and durable concrete.

2. Material and methods

2.1. Raw materials

The Portland cement confirming to the requirement in BS EN 197-1 class 52.5 N (BS En, 2011) was used for concrete production. Five SCMs were used in this study, including two conventional SCMs (FA and GGBS) and three non-conventional SCMs (VA, VA-LS blends, MK-LS blends). All the SCMs except VA were directly used for the production of concretes without preprocessing. The raw VA used in this study was sourced from Indonesia. Before being used to produce concrete specimens, the raw VA was ground using a ball mill and sieved through 150 μm to remove larger particles and other impurities. After that, the VA was dried at 105 °C in an oven for one day. Fig. 1 shows the SEM image of post-processed VA. The VA particles show angular forms with some flocky particles on the surface. The chemical characteristics (measured

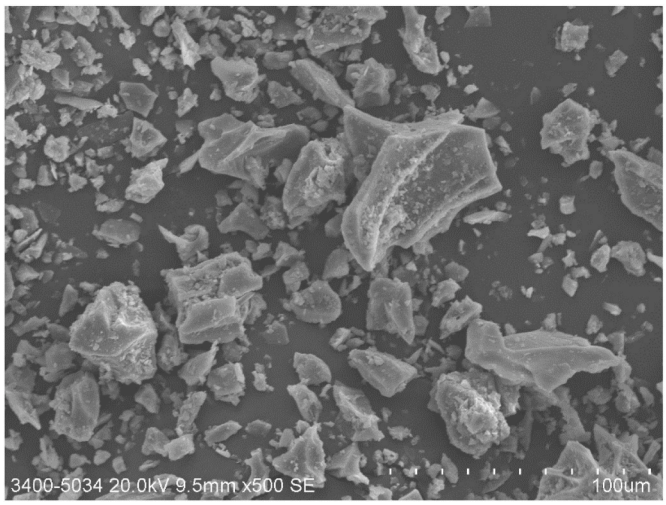

Fig. 1. SEM image of volcanic ash.

Table 1
Chemical characteristics of cement and SCMs.

Oxides (% by mass)	Portland cement CEM I 52.5 N	GGBS	PFA	VA	MK	LS
Na_2O			1.99	1.91		
MgO	0.84	6.33	2.70	0.81		0.95
Al_2O_3	3.95	13.81	20.38	14.86	43.05	0.08
SiO_2	19.88	32.53	50.74	71.73	54.67	
SO_3	5.06	3.16	1.61	0.05		0.07
K_2O	0.57	1.13	1.81	2.41		
CaO	65.54	40.73	9.37	1.84		54.57
TiO_2		1.28	1.15	0.33	0.69	
Fe_2O_3	2.73	0.31	6.19	2.6	0.43	0.03
MnO		0.17	0.14	0.09		
Loss on ignition at 900 °C	1.43	0.54	3.91	3.37	1.15	45.43
Pozzolanic activity (mg of $Ca(OH)_2$ consumed per g of pozzolan)	–	–	545	321	673	–

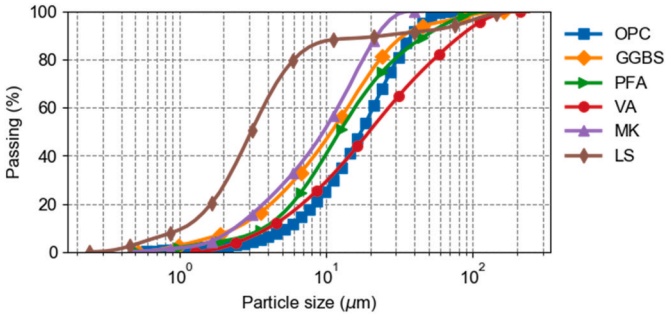

Fig. 2. Particle size distribution of powder materials.

Table 2
Mixture proportions of concrete.

Materials (kg/m^3)	Mixture ID					
	NC	SC	PC	VC	VLC	MLC
Portland cement CEM I 52.5 N	450.0	315.0	315.0	315	315	315
Ground granulated blast furnace slag (GGBS)	0.00	119.4	0.00	0	0	0
Pulverized fly ash (PFA)	0.00	0.00	104.8	0	0	0
Volcanic ash (VA)	0.00	0.00	0.00	109	74.3	0
Metakaolin (MK)	0.00	0.00	0.00	0	0	74.3
Limestone (LM)	0.00	0.00	0.00	0	37.1	37.1
Coarse aggregates	1015	1015	1015	1015	1015	1015
Fine aggregates	745	745	745	745	745	745
Water	198	198	198	198	198	198
w/b mass ratio	0.44	0.46	0.47	0.47	0.46	0.46
w/b volume ratio	1.4	1.4	1.4	1.4	1.4	1.4
Superplasticizer	2.2	2.3	2.0	3.7	3	5.2
Slump (mm)	80	80	85	80	150	75

[Note: NC: normal concrete produced with Portland cement; SC: slag concrete with 30% Portland cement replacement; PC: fly ash concrete with 30% Portland cement replacement; MLC: concrete with 20% and 10% Portland cement replacement with metakaolin and limestone, respectively; VLC: concrete with 20% and 10% Portland cement replacement with volcanic ash and limestone, respectively; VC: natural pozzolana concrete with 30% Portland cement replacement].

by X-ray fluorescence) of the Portland cement, PFA, GGBS, VA, MK and LS are summarized in Table 1. The pozzolanic reactivity in the table was quantified through the modified Chapelle test (Ferraz et al., 2015; Ali et al., 2020). The particle size distribution of the Portland cement, PFA, GGBS, VA, MK and LS, measured by laser diffraction spectroscopy, is shown in Fig. 2. Local granite aggregate with a nominal maximum size of 10 mm was used as coarse aggregate in concrete. Due to the global shortage of river sand (Ashish, 2019), crushed granite aggregate with a fineness modulus of 2.72 instead of river sand was used as fine aggregate in concrete. A third-generation polycarboxylate-based superplasticizer (SP), i.e., MasterGlenium SKY 8588, was used to adjust the workability of concrete.

2.2. Mixture proportions

In this study, six concrete mixtures were cast, in which the binder volume content and aggregate volume content were set as the same. Table 2 shows the mixture proportion of concrete. The NC in Table 2 uses Portland cement as the binder and serves as the reference mixture. The SC, PC, and VC have replaced Portland cement partially by 30% GGBS, PFA and VA by volume, respectively. The VLC has replaced Portland cement partially by 20% VA and 10% LS by volume, and the MLC has replaced Portland cement partially by 20% MK and 10% LS by volume. All the mixture proportions were originally designed to have a roughly constant slump (80 mm). However, during the mixing process of VLC, superplasticizer was overdosed slightly, and consequently a much higher slump (150 mm) was achieved unexpectedly. As shown in Table 2, despite the superplasticizer content for VLC is lower than that of VC, the slump of VLC is larger than the counterpart of VC. This is likely due to the fact that limestone can improve the workability as a result of its small size facilitating filling the interstices between the cement and VA particles that form the skeleton.

2.3. Test specimens, curing conditions and testing details

To characterize the initial and final setting properties of these concrete mixtures, cementitious pastes without aggregates were prepared. The Vicat needle method outlined in ASTM C191 was used to quantify both the initial and final setting times of cementitious pastes (ASTM C191, 2019). Each fresh paste mixture sample was first filled into a conical ring with a height measuring 40 mm, an inside bottom diameter measuring 75 mm, and an inside top diameter measuring 65 mm. The fresh paste underwent periodic penetration tests, in which a Vicat needle measuring 1 mm in diameter was allowed to settle into it.

A range of tests on mechanical and durability performance of these six concrete mixes, *viz.* the compressive strength, splitting tensile strength, flexural strength, rate of absorption of water, chloride diffusion coefficient, and alkali-silica reaction vulnerability, were carried out.

The compressive strength of 100 mm cubic specimens was tested at various ages, including 3, 28, and 56 days, in accordance with BS EN 12390–3 (BS EN 12390-3, 2009). The setup for compressive strength test is shown in Fig. 3(a). The splitting tensile strength test was performed on Φ100 × 200 cylindrical specimens at 3, 28 and 56 days as per BS EN 12390–6 (BS EN 12390-6 Testing hardened concrete, 2009). The setup for the splitting tensile strength test is shown in Fig. 3(b). The loading rate for both the compressive strength test and splitting tensile strength test was set to be 3 kN/s. The flexural tensile strength test was conducted on 100 × 100 × 500 prismatic specimens at 3, 28 and 56 days as per BS

(a) Compressive strength test setup (b) Splitting tensile strength test setup (c) Flexural tensile strength test setup

Fig. 3. Mechanical test setup.

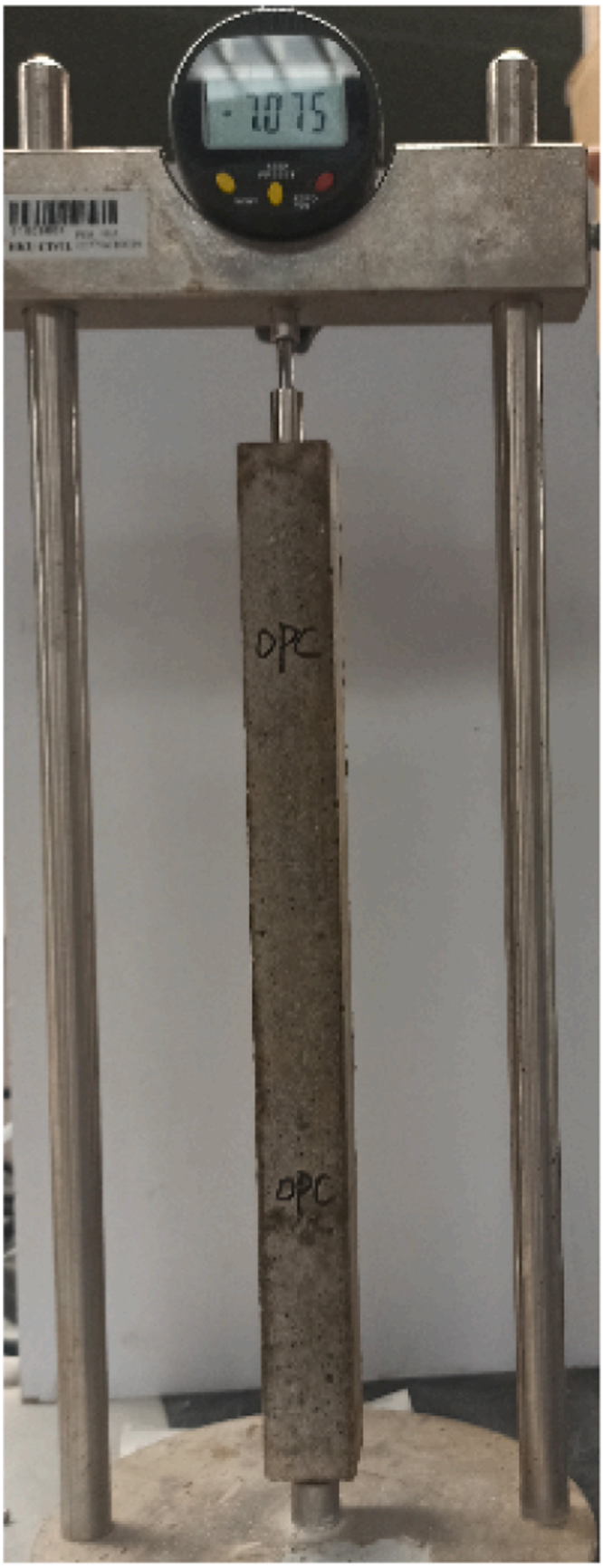

Fig. 4. Apparatus for measurement of length changes.

EN 12390–5 (BS EN, 2009). The flexural strength test setup is shown in Fig. 3(c). The test for flexural strength was conducted with a loading rate of 1 kN/s. Three specimens were tested for each type of mechanical strength test at each age, and the reported values were the average of these tests. After being cast, the specimens were removed from their molds the following day and submerged in a water tank at approximately 23 °C until the time of testing.

The initial and secondary rate of absorption of water of concrete were measured using the Φ100 × 200 cylindrical specimens as per ASTM C1585 (ASTM C1585, 2020). Three duplicate specimens were prepared for each concrete mixture and the mean values were presented. The specimens were removed from the mold after one day of casting and cured in water at around 23 °C for a period of 28 days. The specimens were then taken out of the water tank and cured at a temperature of 50 °C and a relative humidity (RH) of 80% for three days. Subsequently, the specimens were stored in sealed containers (Temperature = ~23 °C and RH = ~65%) for about 56 days before the start of the water absorption test.

Accelerated mortar-bar method was used for determining the potential alkali-silica reactivity of combinations of cementitious materials and aggregate as per ASTM C1567 (ASTM C1567, 2013). The replacement percentages of SCMs in the mortar mixtures were kept the same as those in the concrete mixtures. The main difference of mortar mixtures from concrete mixtures was that, instead of both fine and coarse aggregates, only crushed fine aggregates were used in the mortar mixtures. For each of the six mortar mixtures, three 25 × 25 × 285 mm prismatic specimens were prepared for the accelerated mortar bar test. Two metal gage studs were embedded at the ends of the specimens to facilitate length measurements. A digital length comparator with an measuring precision of 0.001 mm was used to measure the variation in length of the specimens as presented in Fig. 4. The specimens were demolded one day after casting and subsequently immersed in hot water (80 °C) for one day. Following that, the specimens were stored in a 1 M NaOH solution at 80 °C for two more weeks. The length of the specimens was recorded after demolding, 1 day of water bath, and 1, 2, 3, 5, 7, 10 and 14 days of hot NaOH solution bath.

The ASTM C1556 test method was used to determine the resistance of the concrete mixtures against chloride diffusion (ASTM C1556, 2011). Cube specimens, with edges measuring 100 mm, were subjected to NaCl solution with a concentration of 165 g/L. These cubes were cured in water until the age of 28 days. Then, these specimens were stored in room condition for one day to be surface-dry but internally moist (saturated surface-dry state) prior to sealing. All sides of the specimens, except for the bottom surface that would be in contact with the chloride solution, were sealed using epoxy resin. After allowing 24 h for the epoxy to harden, the test specimens were immersed in a saturated lime water bath at 23 ± 2 °C for 3 days in a tightly sealed plastic container. Following saturation, the specimens were transferred to another container and exposed to NaCl solution for 2 months. The unsealed surface of the specimens was positioned facing downwards on plastic grids in the sealed container.

Upon completion of the exposure, powder samples were obtained along the exposure depth by precision grinding with the aid of a profile grinder (Germann Instruments) as shown in Fig. 5. To avoid any contamination from the coated epoxy, the grinding process was applied within the central area of the specimens, which had a diameter of 75 mm. The grinding thicknesses along the depth direction were 0–1, 1–3, 3–5, 5–7, 7–9, 9–12, 12–16 and 16–20 mm, as shown in Fig. 5. Prior to measuring the chloride content, the powders were gathered and stored in labelled sample bags.

Two methods, namely, water-soluble method and acid-soluble method were adopted for measuring chloride contents. Before measuring, the abovementioned collected powder samples were oven-dried at 105 °C for 1 day to eliminate moisture in the concrete powders samples. The acid-soluble chloride content was measured with a method as per ASTM C1152 (ASTM C1152, 2020). A 150 mL glass

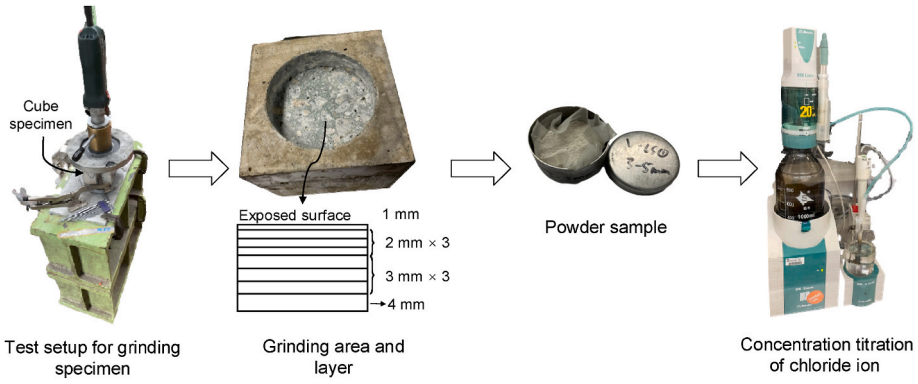

Fig. 5. Measurement of chloride content in concrete.

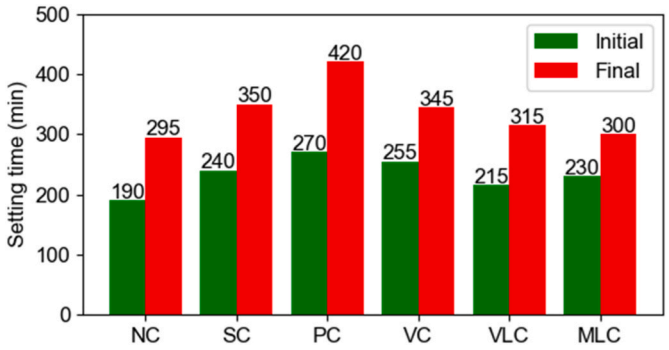

Fig. 6. Initial and final setting times of cementitious binders of the concretes.

beaker was used to measure about 1.5 g of powder sample, to which 20 mL of deionized water was subsequently added. Subsequently, 5 mL of nitric acid (69% concentration) was loaded into the beaker. For SC, VC and VLC, 1 mL of 30% hydrogen peroxide was added to remove the influence of sulfides in concrete. The as-prepared solution was covered and heated until boiling, and then allowed to cool to room temperature. Thereafter, it was filtered out with filter paper and the vial was rinsed using approximately 100 mL of deionized water to guarantee complete collection of chloride ions. The water-soluble chloride content was measured with a method as per ASTM C1218 (ASTM C1218, 2020). A 150 mL glass beaker was used to measure about 1.5 g of powder sample, to which 20 mL of deionized water was subsequently added. The solution was covered and boiled for 5 min. Then the solution was allowed to stand for 24 h at room temperature. After that, the solution went through the filtration procedure just like that for the acid-soluble solution. Subsequently, 1 mL of nitric acid (69% concentration) was loaded into the filtrate. Again, for SC, VC and VLC, 1 mL of 30% hydrogen peroxide was added to remove the influence of sulfides in concrete.

3. Results and discussion

3.1. Setting times

Fig. 6 shows the initial and fine setting times of the binders of the six types of concrete. It is evident from the figure that the incorporation of SCMs into the Portland cement has increased both the initial and final setting times. This is mainly due to the dilution effect of these incorporated SCMs. The setting times of VLC and MLC are closest to those of NC: the initial setting times of VLC and MLC are respectively 25 and 40 min longer than that of NC, and the final setting times of VLC and MLC are respectively 20 and 5 min longer than that of NC. It is noted that 10% of replacement of VA in VC by LS can reduce the initial and final setting times by 40 and 30 min, respectively. The reduction in cement setting times resulting from the inclusion of limestone can be accounted for partially by the seeding and nucleation effects of small particle sizes on the cement hydration process (Wang et al., 2021; Rahhal et al., 2012). The small size of limestone particles allows them to fill the gaps between cement particles, serving as nucleation sites for hydration and subsequently expediting the rate of cement hydration (Wang et al., 2018). Another reason could be the retarding effect of superplasticizer, as more superplasticizer was used in VC than VLC. Among the six cementitious binders, PC has the largest initial and final setting times (270 and 420 min). It should be noted that different dosages of superplasticizer were used in each cementitious mixture. So, the effect of the combinations in setting times includes also the effect of superplasticizer, because superplasticizers normally encompass regarding effects.

3.2. Mechanical strength

3.2.1. Compressive strength

Fig. 7(a) shows the compressive strength development of the six concrete mixtures from an age of 3 days–56 days. The compressive strength of all the six concrete mixtures increases as their ages increase, however, the increase from 28 days to 56 days is relatively small compared to that from 3 days to 28 days. At 3 days, the NC has a compressive strength of 50.1 MPa, which is respectively 10.6, 19.9, 22.3, 19.2 and 6.1 MPa larger than that of SC, PC, VC, VLC, and MLC. This indicates that the addition of SCM, regardless of whether an industrial byproduct or natural pozzolan, could reduce the early-age compressive strength of concrete. Among the five types of concretes with SCMs, VC has the lowest 3-day compressive strength, while MLC has the highest 3-day compressive strength.

The 28-day compressive strengths of the NC, SC, PC, VC, VLC and MLC have increased by 50.8%, 85.2%, 104.8%, 63.7%, 60.5% and 96.1%, respectively, compared to their respective counterparts at 3 days. It is noted that all the concretes with SCMs have a larger increase in compressive strength than the NC, owing to the pozzolanic reaction. The 28-day compressive strength of MLC has reached 86.3 MPa, which tops among the six concrete mixtures. This is probably due to the high pozzolanic reactivity of MK (see Table 1), which promotes the pozzolanic reaction between the pozzolan and calcium hydroxide (CH) especially within 7–14 days (Ashish and Verma, 2019). The high degree of pozzolanic reaction in MLC is evidenced by a very small amount of CH in the MLC binder at 28 days as seen in Fig. 8 and Fig. 9.

Fig. 8 shows the distributions of weight loss percentages of cementitious binders at an age of 28 days at various temperature ranges. These weight losses of cementitious binders were measured by thermogravimetric analysis (TGA) equipment. The TGA was conducted by heating about 50 mg ground cementitious paste sample from 30 °C to 950 °C at 20 °C/min in nitrogen flow (20 mL/min). The weight loss percentage in between 400 °C and 550 °C corresponds to the CH content in the cementitious binder. As shown in Fig. 8, the CH contents in all the five

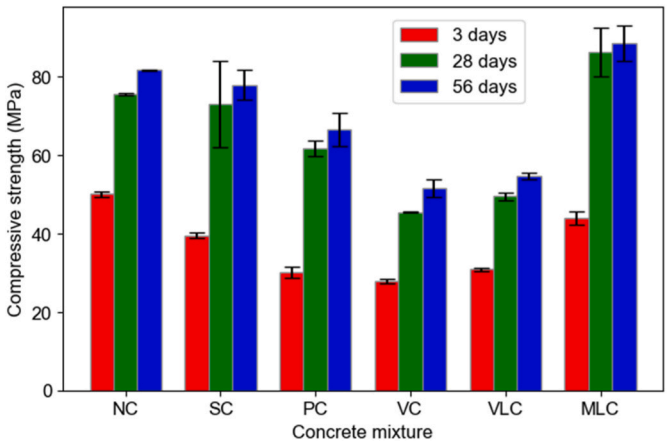

(a) Compressive strength

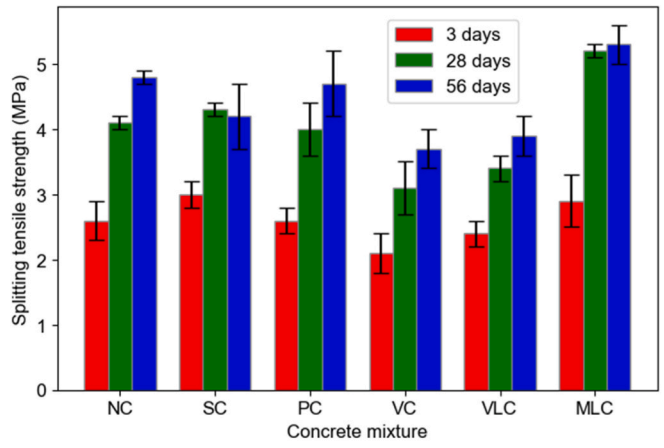

(b) Splitting tensile strength

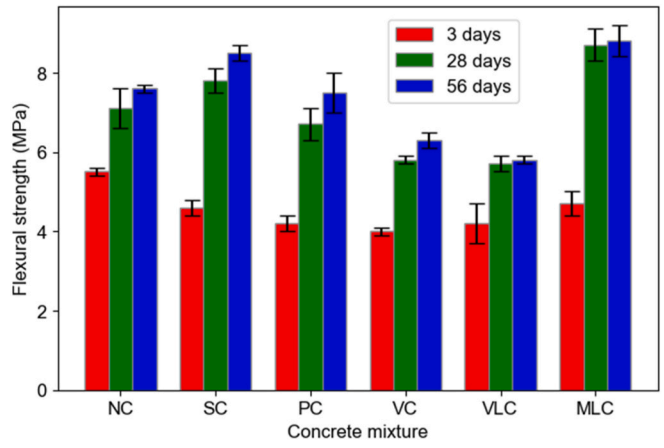

(c) Flexural tensile strength

Fig. 7. Mechanical strength development of the six concrete mixtures.

concrete mixtures containing SCMs are less than that in NC. Furthermore, the CH content in MLC is obviously the lowest. This finding is further confirmed in the XRD diffractograms of these six cementitious binders at an age of 28 days as shown in Fig. 9. As can be seen in the figure, the magnitudes of peaks corresponding to the CH phase are the lowest for the MLC.

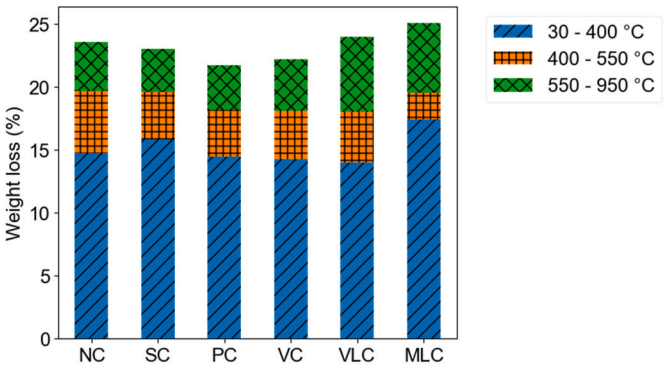

Fig. 8. Distributions of weight loss percentages of cementitious binders at an age of 28 days at various temperature ranges.

The 28-day compressive strengths of NC and SC are comparable and respectively 10.8 MPa and 13.2 MPa smaller than that of MLC. The 28-day compressive strength of PC is in between those of SC and VLC, i.e., 11.3 MPa lower than that of SC and 12.2 MPa higher than that of VLC. The compressive strengths of VLC and VC are considerably lower than those of other concrete mixtures. This is likely a result of the considerably low pozzolanic reactivity of VA as opposed to those of PFA and MK (see Table 1). This relatively low pozzolanic reactivity of the used VA may be partially attributed to its coarsest particle size, as evidenced in Fig. 2. At 56 days, no remarkable changes are observed in compressive strengths of the six concrete mixtures compared to the counterparts at 28 days.

3.2.2. *Splitting tensile strength*

Fig. 7(b) shows the splitting tensile strength development of the six concrete mixtures from an age of 3 days–56 days. The splitting tensile strengths of all the six concrete mixtures increase as their ages increase except for SC, which shows a marginally slight reduction from 28 days to 56 days. The 3-day splitting tensile strengths of NC, SC, PC, VC, VLC and MLC are 2.6, 3.0, 2.6, 2.1, 2.4 and 2.9 MPa, respectively. At 28 days, the splitting tensile strengths of NC, SC, PC, VC, VLC and MLC increase by 57.7%, 43.3%, 53.8%, 47.6%, 41.7% and 79.3%, respectively, compared to their respective counterparts at 3 days. It is noted that the splitting tensile strength of MLC is the highest and that of VC is the lowest among the six concrete mixtures. A slight different from the trend in compressive strength, the splitting tensile strengths of SC and PC at 3, 28 and 56 days are comparable to that of NC, and the splitting tensile strength of MLC is higher than that of NC at 3, 28 and 56 days. It is well-known that there exists a strong correlation between compressive strength and splitting tensile strength of concrete. Different codes have provided different empirical formulas for the relationship between them, as summarized in Table 3. Fig. 10 compares the as-obtained test data to the established formulas in different codes. As seen from the figure, the formula proposed by fib model code 2010 (fib, 2013) gives the best prediction with a coefficient of determination (R^2) of 0.863, followed closely by ACI 318 formula (ACI 318R, 2014) with $R^2 = 0.820$.

3.2.3. *Flexural strength*

Fig. 7(c) shows the flexural strength development of the six concrete mixtures from 3 day to 56 day. The flexural strength of all the six concrete mixtures increases as their ages increase, but the increase from 28 days to 56 days is minimal. At 3 days, NC has the highest flexural tensile strength, followed by MLC, SC, PC, VLC and VC. At 28 days, the flexural tensile strengths of NC, SC, PC, VC, VLC and MLC have increased by 29.1%, 69.6%, 59.5%, 45.0%, 35.7% and 85.1%, respectively, compared to their respective counterparts at 3 days. MLC has the highest flexural tensile strength at 28 days and 56 days. The flexural tensile strengths of VC and VLC remain to be the two lowest throughout the

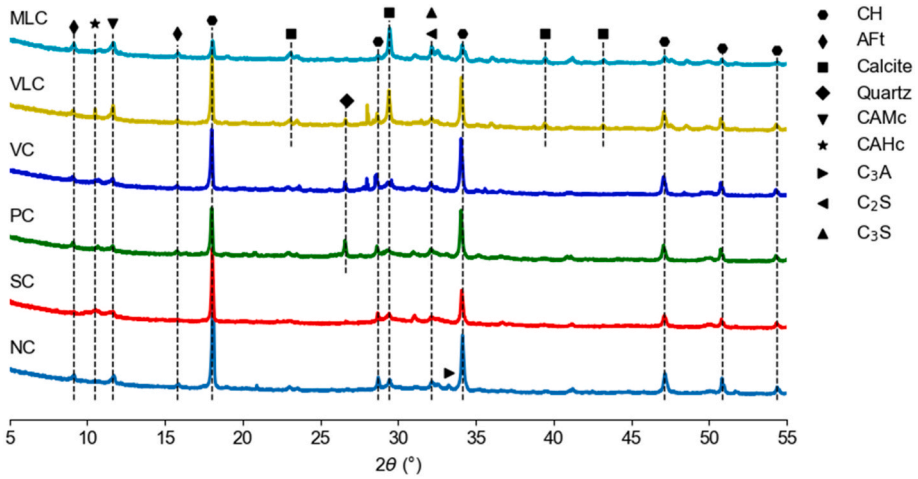

Fig. 9. XRD diffractograms of cementitious binders at an age of 28 days.

Table 3
Empirical formulas between compressive, splitting tensile and flexural tensile strength of concrete in different codes.

Relationship between compressive and splitting tensile strength		Relationship between compressive and flexural tensile strength	
Reference	Formula	Reference	Formula
ACI 318–2014 (ACI 318R, 2014)	$f_{st} = 0.56(f_{c,cy})^{0.5}$	ACI 318–2014 (ACI 318R, 2014)	$f_{ft} = 0.62(f_{c,cy})^{0.5}$
ACI 363R-92 (ACI 363R-92, 1992)	$f_{st} = 0.59(f_{c,cy})^{0.5}$	ACI 363R-92 (ACI 363R-92, 1992)	$f_{ft} = 0.94(f_{c,cy})^{0.5}$
Fib model code-2010 (fib, 2013)	$f_{st} = 0.3(f_{c,cy})^{0.67}$	AS 3600–2009 (AS 3600, 2009)	$f_{ft} = 0.6(f_{c,cy})^{0.5}$
AS 3600–2009 (AS 3600, 2009)	$f_{st} = 0.4(f_{c,cy})^{0.5}$	IS 456–2000 (IS 456, 2000)	$f_{ft} = 0.7(f_{c,cu})^{0.5}$
JCI-2008 (JCI, 2008)	$f_{st} = 0.13(f_{c,cy})^{0.85}$		
JSCE-2007 (JSCE and Guidelines for Concrete, 2007)	$f_{st} = 0.23(f_{c,cy})^{0.67}$		

[Note: f_{st} denotes splitting tensile strength of concrete, f_{ft} denotes flexural tensile strength of concrete, sometimes also called modulus of rupture, $f_{c,cy}$ denotes cylinder compressive strength of concrete, $f_{c,cu}$ denotes cube compressive strength of concrete, and $f_{c,cy}$ is commonly taken as 80% of $f_{c,cu}$.].

testing period. Some codes have provided different empirical formulas for calculating flexural tensile strength or sometimes called modulus of rupture given compressive strength of concrete, as summarized in Table 3. Fig. 11 plots the experimental data in this study against the established formulas in different codes. As seen from the figure, the formula proposed by ACI 363R (ACI 363R-92, 1992) gives the most accurate predictions with $R^2 = 0.866$, notably higher than the rest three formulas.

3.3. Durability properties

3.3.1. Rate of water absorption

Fig. 12 shows the initial and secondary rates of absorption of water of the six concrete mixtures. VC has the highest initial rate of absorption of water, followed by VLC, PC, NC, SC and MLC. The substitution of cement by VA and PFA has increased the initial rate of absorption of water of concrete, while the substitution of cement by GGBS and MK/LS has decreased the initial rate of absorption of water of concrete. However, the replacement of cement by PFA has decreased the secondary rate of absorption of water of concrete. VC has the highest secondary rate of absorption of water, followed by VLC, NC, SC, PC and MLC. It is noted that both the initial and secondary rates of water absorption of MLC are much smaller than those of the control mixture, i.e., NC. The initial rate of water absorption of MLC is 16.7% that of NC, and the secondary rate of water absorption of MLC is 37.1% of that of NC.

3.3.2. Alkali-silica reaction

Fig. 13 displays the expansion of the six concrete mixtures throughout the entire period of the accelerated mortar bar test. It is noted that VC and VLC show an obvious shrinkage behavior during the first week. Their shrinkage values peak at the 5th days, and have then gradually increased as testing age increases. All the recorded maximum expansion values of the six concrete mixtures are far below the ASTM threshold expansion value (0.1%), as shown in the figure. This indicates that all the six concrete mixtures containing the granite aggregates are not vulnerable to ASR. Among the six mixtures, the expansion values of NC and SC at 14 days are the two highest, while the expansion values of the rest four concrete mixtures are minimal at 14 days.

3.3.3. Chloride diffusion coefficient

Potentiometric titration was used to measure the acid-soluble and water-soluble chloride contents via a Metrohm Titrando 905 titrator using 0.1 M $AgNO_3$. The chloride concentration was computed by:

$$Cl[wt.\%] = \frac{3.545 \cdot V \cdot N \cdot T}{m} \quad (1)$$

in which V is the volume (mL) of the used $AgNO_3$ solution, N is the concentration of the used $AgNO_3$ solution, = 0.1 M in this case, T represents the titer between the actual concentration and the nominal concentration, and m denotes the mass of powder sample (gram).

By fitting Eq. (2) with the acid-soluble chloride content measured in accordance with ASTM C1556, the apparent chloride diffusion coefficient of concrete was determined following the bulk diffusion test (ASTM C1556, 2011). Similarly, the effective chloride diffusion coefficient of concrete was determined by fitting Eq. (2) with the measured water-soluble chloride content.

$$C(x,t) = C_s - (C_s - C_i) \cdot erf\left(\frac{x}{\sqrt{4 \cdot D \cdot t}}\right) \quad (2)$$

where $C(x,t)$ denotes chloride content measured at exposure time t and depth x. C_s denotes the chloride concentration at the boundary between specimen and the liquid, C_i denotes the initial chloride concentration of the concrete specimen before submersion in the liquid, x denotes the depth from exposed face to the midpoint of a given layer in m, t denotes the exposure period in s, D denotes either apparent or effective chloride diffusion coefficient of concrete calculated from acid-soluble chloride

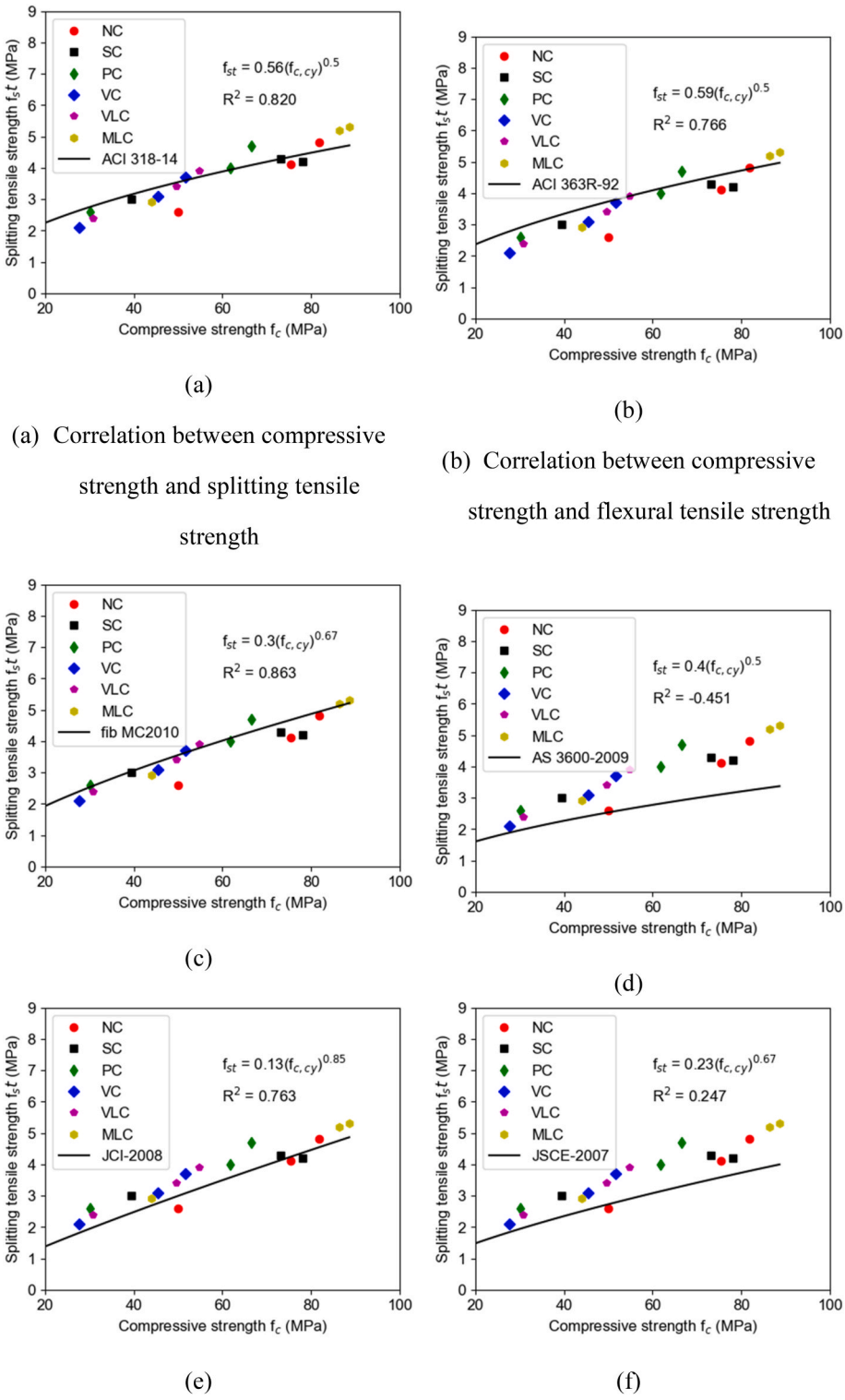

(a) Correlation between compressive strength and splitting tensile strength

(b) Correlation between compressive strength and flexural tensile strength

Fig. 10. Relationship between compressive strength and splitting tensile strength of concretes: experimental data vs. empirical formulas in different codes.

profile or water-soluble chloride profile, respectively, and *erf* denotes the error function.

Fig. 14 shows the acid-soluble and water-soluble chloride content distributions within the concrete specimens along the direction perpendicular to the exposed face. As displayed in Fig. 14(a), the acid-soluble chloride concentrations of the MLC concrete sample at 2, 4, 6 and 8.5 mm are obviously smaller than that of those of the other concrete samples. The acid-soluble chloride concentrations of the NC sample at 6, 8.5,11.5 and 14.5 mm are obviously larger than that of those of the other concrete samples. The acid-soluble chloride contents of VC and VLC are close, and the acid-chloride contents of SC and PC are similar. And the former are higher than the latter. Similar findings can be observed from Fig. 14(b) for the case of the water-soluble chloride profiles.

Fig. 15 plots the acid-soluble chloride concentrations versus the water-soluble concentrations at various layers of concrete mixtures after

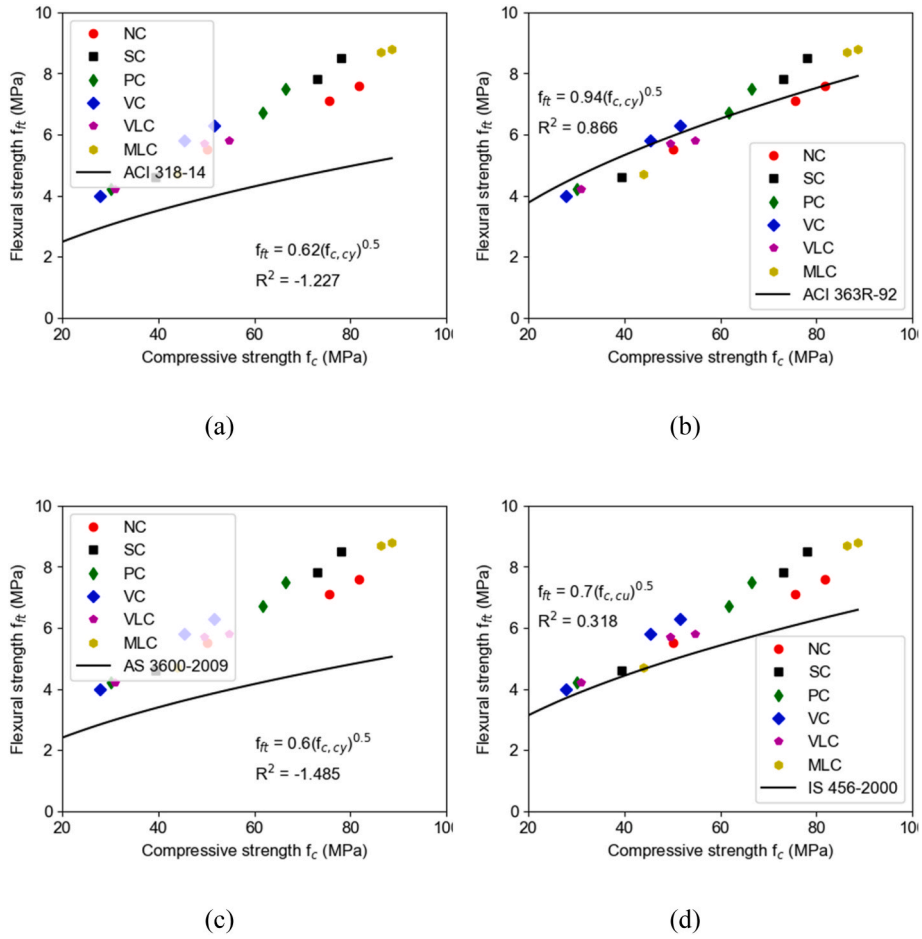

Fig. 11. Relationship between compressive strength and flexural tensile strength of concretes: experimental data vs. empirical formulas in different codes.

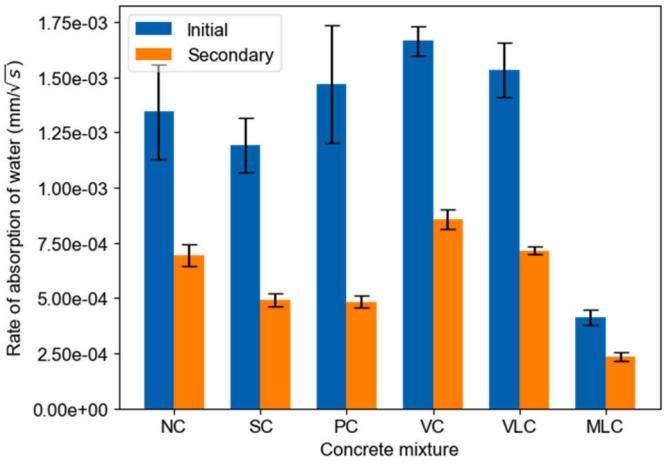

Fig. 12. Initial and secondary rates of absorption of water of the six concrete mixtures.

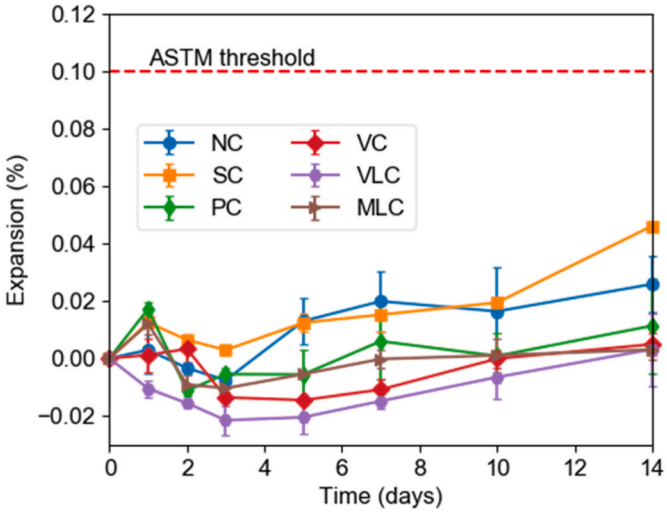

Fig. 13. ASR expansion of the six concrete mixtures.

the bulk diffusion test. As seen from this figure, there is a good linear correlation between the acid-soluble content and water-soluble content. The acid-soluble chloride content is about 1.147 times the acid-soluble chloride content, indicating a small portion of chloride ions are chemically bound by the cementitious binders of concrete.

Fig. 16 compares the apparent and effective chloride diffusion coefficients of the six concrete mixtures determined based on the acid-soluble and water-soluble chloride measurements. The apparent chloride diffusion coefficient of NC is obviously greater than those of the others, indicating that addition of SCMs, i.e., GGBS, PFA, VA or MK, is reducing the apparent chloride diffusion coefficient. This is due to the pozzolanic reactions between the pozzolan and calcium hydroxide, which has refined the pore structure and as a consequence has decreased the chloride diffusivity of concrete. But the effectiveness of SCMs in reducing the chloride diffusion coefficient is different, as displayed in

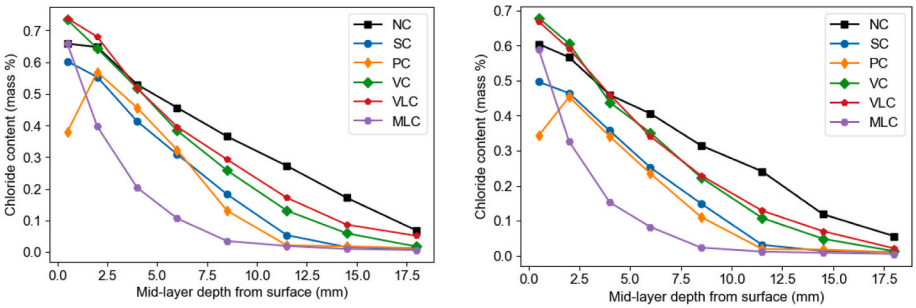

Fig. 14. Chloride profiles of concrete mixtures diffused in NaCl solution.

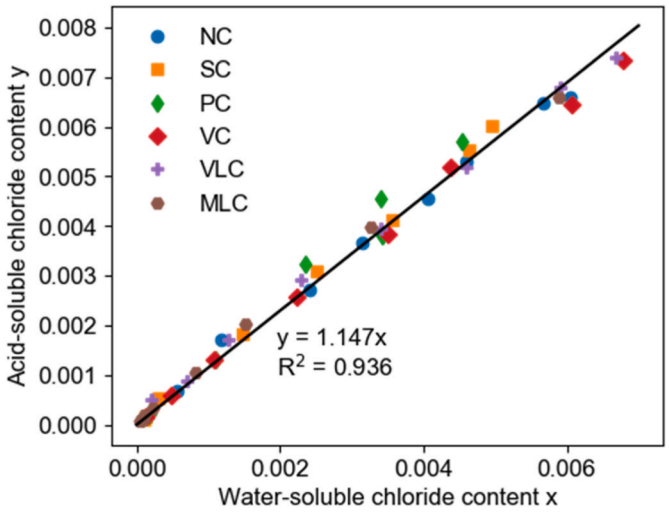

Fig. 15. Acid-soluble chloride content versus water-soluble content in all layers of concrete mixtures after chloride diffusion test.

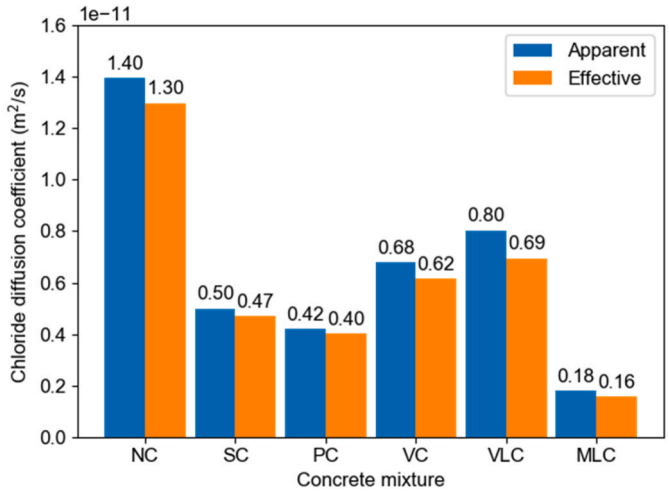

Fig. 16. Apparent and Effective chloride diffusion coefficients of concrete mixtures.

Fig. 16. The apparent chloride diffusion coefficient of VC is about half of that of NC. Addition of limestone in concrete with volcanic ash has increased its apparent chloride diffusion coefficient slightly. The apparent chloride diffusion coefficients of PC and SC are close, both smaller than that of VC and larger than that of MLC. The apparent chloride diffusion coefficient of MLC is the smallest among all the six concrete mixtures, which is only about one eighth of the NC counterpart. This difference originates from the different pozzolanic reactivity of the pozzolans listed in Table 1. Similar findings can be observed for the effective chloride diffusion coefficients of concrete. Based on the effective chloride diffusion coefficient, the chloride penetration resistance of concrete can be categorized into five grades: low, moderate, high, very high and extremely high, as shown in Table 4. It can be concluded from Fig. 16 and Table 4 that the chloride penetration resistance of these six concrete mixtures ranges from moderate (NC) to, high (VC, VLC), very high (SC, PC), and extremely high (MLC).

Table 4
Resistance against chloride penetration based on non-steady state migration testing (Gjørv, 2009).

Chloride diffusion coefficient D ($\times 10^{-12}$ m^2/s)	>15	10–15	5–10	2.5–5	<2.5
Concrete resistance	Low	Moderate	High	Very high	Extremely high
Concrete mixture		NC	VC, VLC	SC, PC	MLC

4. Conclusions and outlook

With concerns over the future availability of PFA and GGBS, researchers have highlighted the need to identify and promote alternative SCMs to ensure sustainable concrete production. The fresh, mechanical, and durability properties of concrete containing two commonly used SCMs and three emerging potential ones, were evaluated comparatively in this study. The following findings can be obtained from this study:

(1) VA reduces the workability of concrete, and it therefore requires more superplasticizer than the reference ordinary Portland cement concrete to achieve the same slump. However, partial replacement of VA by limestone powder can increase the workability of concrete and reduce the superplasticizer dosage to satisfy workability requirement.
(2) Setting time results show an increase in both the initial and final setting times of the cementitious paste with 30% vol. of Portland cement substitution by SCMs. The VLC binder has the lowest initial setting time followed by MLC, SC, VC and PC in ascending order; the MLC binder has the lowest final setting time followed by VLC, VC, SC and PC in ascending order.
(3) The substitution of 30% vol. of Portland cement by SCMs reduces the early age compressive strength of concrete to different extents. As the maturity age increases upon 56 days, the compressive strengths of PC, VC, and VLC remain obviously lower than that of NC; but the compressive strength of SC has become very

close to that of NC, and for MLC, its 28-day and 56-day compressive strengths are even slightly larger than the counterparts of NC.

(4) The initial and secondary rates of water absorption of MLC and SC are lower than the counterparts of NC, and the initial and secondary rates of water absorption of VC are higher than that of NC. The initial rate of water absorption of PC is larger than that of NC, while its secondary rate of water absorption is smaller than that of NC. Both the initial and secondary rates of water absorption of VLC are slightly smaller than those of VC, indicating that the partial replacement of VA by limestone powder would reduce the water absorption capacity of concrete. MLC has the lowest initial and secondary rates of water absorption, which are about 31% and 34% of the respective counterpart of NC.

(5) There is no risk of ASR expansion in all the six concretes containing granite aggregate. Partial replacement of Portland cement by PFA, VA or MK obviously reduces the ASR expansion, while in contrast, the replacement of Portland cement by GGBS is not effective in controlling the ASR expansion of concrete.

(6) Substitution of 30% vol. of Portland cement by SCMs decreases the chloride diffusion coefficient of concrete and thereby increases the ability of concrete against chloride ingress to different extents. MLC has the smallest chloride diffusion coefficient followed by PC, SC, VC and VLC in ascending order. It should be noted that the addition of VA reduces the mechanical strength of concrete, but it still increases concrete's ability to resist chloride ingress.

The present study only covers a part of the fresh, mechanical, and durability properties of concrete, and thus, future works are recommended to compare the ordinary Portland cement containing these SCMs in terms of their (1) thixotropic behavior; (2) sulfate resistance; (3) acid resistance; (4) long-term shrinkage and creep; (5) freeze-thaw resistance; (6) antimicrobial performance; and (7) self-healing potentials. Filling in these research gaps would further inform engineers of the strengths and potential weaknesses of these green concretes and help them make decisions on choosing suitable SCMs based on the technical requirements.

Declaration of competing interest

The authors declare that they have no known competing financial interests or personal relationships that could have appeared to influence the work reported in this paper.

Data availability

The authors do not have permission to share data.

Acknowledgements

The authors would like to thank the Environment and Ecology Bureau of the Government of Hong Kong SAR for financially supporting this project through the Green Tech Fund (Grant No.: GTF202110158). Besides, Peakward Enterprises (Holdings) Ltd., Hong Kong is gratefully acknowledged for supplying the raw volcanic ash.

References

ACI 318R-14, Building Code Requirements for Structural Concrete (ACI 318-14) and Commentary on Building Code Requirements for Structural Concrete, 2014. Farmington Hills, Michigan.

ACI 363R-92, 1992. State of the Art Report on High-Strength Concrete. Detroit, MI.

Al-Fadala, S., Chakkamalayath, J., Al-Bahar, S., Al-Aibani, A., Ahmed, S., 2017. Significance of performance based specifications in the qualification and characterization of blended cement using volcanic ash. Construct. Build. Mater. 144, 532–540. https://doi.org/10.1016/j.conbuildmat.2017.03.180.

Ali, H.A., Xuan, D., Poon, C.S., 2020. Assessment of long-term reactivity of initially lowly-reactive solid wastes as supplementary cementitious materials (SCMs). Construct. Build. Mater. 232, 117192 https://doi.org/10.1016/j.conbuildmat.2019.117192.

AS 3600-2009: Concrete Structures, 2009. C.S. Standards Association of Australia.

Ashish, D.K., 2019. Concrete made with waste marble powder and supplementary cementitious material for sustainable development. J. Clean. Prod. 211, 716–729. https://doi.org/10.1016/j.jclepro.2018.11.245.

Ashish, D.K., Verma, S.K., 2019. Cementing efficiency of flash and rotary-calcined metakaolin in concrete. J. Mater. Civ. Eng. 31 (12), 04019307 https://doi.org/10.1061/(ASCE)MT.1943-5533.0002953.

Ashish, D.K., Verma, S.K., Ju, M., Sharma, H., 2023. High volume waste foundry sand self-compacting concrete–Transitioning industrial symbiosis. Process Saf. Environ. Protect. 173, 666–692. https://doi.org/10.1016/j.psep.2023.03.028.

ASTM C1152, 2020. Standard Test Method for Acid-Soluble Chloride in Mortar and Concrete. West Conshohocken, PA.

ASTM C1218, 2020. Standard Test Method for Water-Soluble Chloride in Mortar and Concrete. West Conshohocken, PA.

ASTM C1556, 2011. Standard Test Method for Determining the Apparent Chloride Diffusion Coefficient of Cementitious Mixtures by Bulk Diffusion. West Conshohocken, PA.

ASTM C1567, 2013. Standard Test Method for Determining the Potential Alkali-Silica Reactivity of Combinations of Cementitious Materials and Aggregate (Accelerated Mortar-Bar Method). West Conshohocken, PA.

ASTM C1585, 2020. Standard Test Method for Measurement of Rate of Absorption of Water by Hydraulic-Cement Concretes. West Conshohocken, PA.

ASTM C191, 2019. Standard Test Methods for Time of Setting of Hydraulic Cement by Vicat Needle. www.astm.org. West Conshohocken, PA.

de Brito, J., Kurda, R., 2021. The past and future of sustainable concrete: a critical review and new strategies on cement-based materials. J. Clean. Prod. 281, 123558 https://doi.org/10.1016/j.jclepro.2020.123558.

BS EN 12390-3, 2009. Testing Hardened Concrete. Compressive Strength of Test Specimens. British Standard Institution (BSI), London, England.

BS EN 12390-6, Testing hardened concrete, 2009. Tensile Splitting Strength of Test Specimens. British Standard Institution (BSI), London, England.

BS EN, 2009. 12390-5 Testing Hardened Concrete–Part 5: Flexural Strength of Test Specimens. British Standard Institution (BSI), London, England.

BS En, 197-1, Cement, Composition, Specifications and Conformity Criteria for Common Cements, 2011. British Standard Institution (BSI), London, England.

Dhandapani, Y., Sakthivel, T., Santhanam, M., Gettu, R., Pillai, R.G., 2018. Mechanical properties and durability performance of concretes with limestone calcined clay cement (LC3). Cement Concr. Res. 107, 136–151. https://doi.org/10.1016/j.cemconres.2018.02.005.

Du, H., Dai Pang, S., 2020. High-performance concrete incorporating calcined kaolin clay and limestone as cement substitute. Construct. Build. Mater. 264, 120152 https://doi.org/10.1016/j.conbuildmat.2020.120152.

Elahi, A., Basheer, P., Nanukuttan, S., Khan, Q., 2010. Mechanical and durability properties of high performance concretes containing supplementary cementitious materials. Construct. Build. Mater. 24 (3), 292–299. https://doi.org/10.1016/j.conbuildmat.2009.08.045.

Fan, C., Miller, S.A., 2018. Reducing greenhouse gas emissions for prescribed concrete compressive strength. Construct. Build. Mater. 167, 918–928. https://doi.org/10.1016/j.conbuildmat.2018.02.092.

Ferraz, E., Andrejkovičová, S., Hajjaji, W., Velosa, A.L., Silva, A.S., Rocha, F., 2015. Pozzolanic activity of metakaolins by the French Standard of the modified Chapelle Test: a direct methodology. Acta Geodyn. Geomater. 12 (3), 289–298. https://doi.org/10.13168/AGG.2015.0026.

fib, 2013. Model Code for Concrete Structures 2010. Ernst and Son.

Gholampour, A., Ozbakkaloglu, T., 2017. Performance of sustainable concretes containing very high volume Class-F fly ash and ground granulated blast furnace slag. J. Clean. Prod. 162, 1407–1417. https://doi.org/10.1016/j.jclepro.2017.06.087.

Gholampour, A., Zheng, J., Ozbakkaloglu, T., 2021. Development of waste-based concretes containing foundry sand, recycled fine aggregate, ground granulated blast furnace slag and fly ash. Construct. Build. Mater. 267, 121004 https://doi.org/10.1016/j.conbuildmat.2020.121004.

Gjørv, O.E., 2009. Durability Design of Concrete Structures in Severe Environments. CRC Press.

Hafez, H., Kurda, R., Cheung, W.M., Nagaratnam, B., 2020. Comparative life cycle assessment between imported and recovered fly ash for blended cement concrete in the UK. J. Clean. Prod. 244, 118722 https://doi.org/10.1016/j.jclepro.2019.118722.

Hossain, K.M., Lachemi, M., 2006. Development of volcanic ash concrete: strength, durability, and microstructural investigations. ACI Mater. J. 103 (1), 11. https://doi.org/10.14359/15122.

Hossain, K.M.A., Lachemi, M., 2007. Strength, durability and micro-structural aspects of high performance volcanic ash concrete. Cement Concr. Res. 37 (5), 759–766. https://doi.org/10.1016/j.cemconres.2007.02.014.

Hossain, M.U., Liu, J.-C., Xuan, D., Ng, S.T., Ye, H., Abdulla, S.J., 2022. Designing sustainable concrete mixes with potentially alternative binder systems: multicriteria decision making process. J. Build. Eng. 45, 103587 https://doi.org/10.1016/j.jobe.2021.103587.

IS 456, Code of Practice for Plain and Reinforced Cement Concrete, 2000. Bureau of Indian Standards New Delhi, India.

Jackson, M., Deocampo, D., Marra, F., Scheetz, B., 2010. Mid-Pleistocene pozzolanic volcanic ash in ancient Roman concretes. Geoarchaeology: Int. J. 25 (1), 36–74. https://doi.org/10.1002/gea.20295.

Jackson, M.D., Landis, E.N., Brune, P.F., Vitti, M., Chen, H., Li, Q., Kunz, M., Wenk, H.-R., Monteiro, P.J., Ingraffea, A.R., 2014. Mechanical resilience and cementitious processes in Imperial Roman architectural mortar. Proc. Natl. Acad. Sci. USA 111 (52), 18484–18489. https://doi.org/10.1073/pnas.1417456111.

JCI, 2008. Guidelines for Control of Cracking of Mass Concrete. Japan Concrete Institute Tokyo, Japan.

JSCE, Guidelines for Concrete, 2007. Standard Specifications for Concrete Structures. Japan Society of Civil Engineers.

Lemougna, P.N., Wang, K.-t., Tang, Q., Nzeukou, A., Billong, N., Melo, U.C., Cui, X.-m., 2018. Review on the use of volcanic ashes for engineering applications. Resour. Conserv. Recycl. 137, 177–190. https://doi.org/10.1016/j.resconrec.2018.05.031.

Liu, Z., Takasu, K., Koyamada, H., Suyama, H., 2022. A study on engineering properties and environmental impact of sustainable concrete with fly ash or GGBS. Construct. Build. Mater. 316, 125776 https://doi.org/10.1016/j.conbuildmat.2021.125776.

Maddalena, R., Taha, H., Gardner, D., 2021. Self-healing potential of supplementary cementitious materials in cement mortars: sorptivity and pore structure. Developments in the built environment 6, 100044. https://doi.org/10.1016/j.dibe.2021.100044.

De Maeijer, P.K., Craeye, B., Snellings, R., Kazemi-Kamyab, H., Loots, M., Janssens, K., Nuyts, G., 2020. Effect of ultra-fine fly ash on concrete performance and durability. Construct. Build. Mater. 263, 120493 https://doi.org/10.1016/j.conbuildmat.2020.120493.

Meddah, M.S., 2015. Durability performance and engineering properties of shale and volcanic ashes concretes. Construct. Build. Mater. 79, 73–82. https://doi.org/10.1016/j.conbuildmat.2015.01.020.

Mehta, A., Ashish, D.K., 2020. Silica fume and waste glass in cement concrete production: a review. J. Build. Eng. 29, 100888 https://doi.org/10.1016/j.jobe.2019.100888.

Nguyen, Q.D., Khan, M.S.H., Castel, A., 2018. Engineering properties of limestone calcined clay concrete. J. Adv. Concr. Technol. 16 (8), 343–357. https://doi.org/10.3151/jact.16.343.

Nguyen, Q.D., Afroz, S., Zhang, Y., Kim, T., Li, W., Castel, A., 2022. Autogenous and total shrinkage of limestone calcined clay cement (LC3) concretes. Construct. Build. Mater. 314, 125720 https://doi.org/10.1016/j.conbuildmat.2021.125720.

Nickovic, S., Vukovic, A., Vujadinovic, M., Djurdjevic, V., Pejanovic, G., 2012. High-resolution mineralogical database of dust-productive soils for atmospheric dust modeling. Atmos. Chem. Phys. 12 (2), 845–855. https://doi.org/10.5194/acp-12-845-2012.

Nighot, N.S., Kumar, R., 2023. A comprehensive study on the synthesis and characterization of eco-cementitious binders using different kind of industrial wastes for sustainable development. Developments in the Built Environment 14, 100135. https://doi.org/10.1016/j.dibe.2023.100135.

Rahhal, V., Bonavetti, V., Trusilewicz, L., Pedrajas, C., Talero, R., 2012. Role of the filler on Portland cement hydration at early ages. Construct. Build. Mater. 27 (1), 82–90. https://doi.org/10.1016/j.conbuildmat.2011.07.021.

Scrivener, K., Martirena, F., Bishnoi, S., Maity, S., 2018. Calcined clay limestone cements (LC3). Cement Concr. Res. 114, 49–56. https://doi.org/10.1016/j.cemconres.2017.08.017.

Seymour, L.M., Maragh, J., Sabatini, P., Di Tommaso, M., Weaver, J.C., Masic, A., 2023. Hot mixing: mechanistic insights into the durability of ancient Roman concrete. Sci. Adv. 9 (1), eadd1602 https://doi.org/10.1126/sciadv.add1602.

Sharma, M., Bishnoi, S., Martirena, F., Scrivener, K., 2021. Limestone calcined clay cement and concrete: a state-of-the-art review. Cement Concr. Res. 149, 106564 https://doi.org/10.1016/j.cemconres.2021.106564.

Siddique, R., 2012. Properties of concrete made with volcanic ash. Resour. Conserv. Recycl. 66, 40–44. https://doi.org/10.1016/j.resconrec.2012.06.010.

da Silva Magalhães, M., Cezar, B.F., Lustosa, P.R., 2023. Influence of Brazilian Fly Ash Fineness on the Cementing Efficiency Factor, Compressive Strength and Young's Modulus of Concrete, Developments in the Built Environment, 100147. https://doi.org/10.1016/j.dibe.2023.100147.

Soutsos, M., Vollpracht, A., Kanavaris, F., 2020. Applicability of fib model code's maturity function for estimating the strength development of GGBS concretes. Construct. Build. Mater. 264, 120157 https://doi.org/10.1016/j.conbuildmat.2020.120157.

Tavasoli, S., Nili, M., Serpoush, B., 2018. Effect of GGBS on the frost resistance of self-consolidating concrete. Construct. Build. Mater. 165, 717–722. https://doi.org/10.1016/j.conbuildmat.2018.01.027.

Wang, D., Shi, C., Farzadnia, N., Shi, Z., Jia, H., Ou, Z., 2018. A review on use of limestone powder in cement-based materials: mechanism, hydration and microstructures. Construct. Build. Mater. 181, 659–672. https://doi.org/10.1016/j.conbuildmat.2018.06.075.

Wang, H., Hou, P., Li, Q., Adu-Amankwah, S., Chen, H., Xie, N., Zhao, P., Huang, Y., Wang, S., Cheng, X., 2021. Synergistic effects of supplementary cementitious materials in limestone and calcined clay-replaced slag cement. Construct. Build. Mater. 282, 122648 https://doi.org/10.1016/j.conbuildmat.2021.122648.